Nuclear Physics A385 (1982) 204–220


# MULTILEVEL CALCULATIONS IN ODD-MASS NUCLEI (I). Negative-parity states

M.A. CUNNINGHAM*

*A. W. Wright Nuclear Structure Laboratory, Yale University, New Haven, CT 06511, USA*

Received 8 March 1982

**Abstract:** We present the results of an analysis of the negative-parity states in the odd-mass transitional isotopes of xenon and barium, within the framework of the interacting boson-fermion model. We compare the predictions of a simple, single $j$-orbit calculation including the $1h_{11/2}$ orbital with those of a multilevel approach. Our findings indicate that the low-lying collective structures in these nuclei are strongly influenced by admixtures of higher-lying single-particle degrees of freedom, notably the $2f_{7/2}$ and $1h_{9/2}$ levels.

## 1. Introduction

The low-lying collective structures in transitional, odd-mass nuclei have been investigated experimentally in some detail in recent years. However, detailed, theoretical descriptions of these nuclei were not available; due largely to the fact that these nuclei cannot be readily classified within the framework of simple theoretical models such as the Nilsson model [1]) or the particle-vibration model [2]). Recently, some effort has been made to provide more sophisticated descriptions of these low-lying states [3–5]), which rely on more complicated descriptions of the underlying even-even core nuclei. However, these calculations are generally restricted to the study of unique-parity states based on a single $j$-orbit such as the $1g_{9/2}$ or $1h_{11/2}$. In this report, we shall examine the application of an alternative description of the low-lying collective structures in these nuclei—that of the interacting boson-fermion model [6,7]). As we shall attempt to demonstrate, this model can provide relatively simple, yet accurate, descriptions of these transitional nuclei, but more importantly, it is not restricted to the case where the odd nucleon must occupy only one single-particle orbital. This last feature – the straightforward inclusion of several fermion degrees of freedom – is crucial in determining the structure of the low-lying collective states.

This paper represents the first part of our analysis of the collective states in the light isotopes of xenon and barium. In this report, we shall focus on the high-spin, negative-parity states, which can be thought of as originating from the $1h_{11/2}$ neutron orbital. However, other levels, most notably the $2f_{7/2}$ and $1h_{9/2}$ orbitals,

* Current address: Schlumberger Well Services, P.O. Box 2175, Houston, TX 77001, USA.

could play some role in determining the properties of these negative-parity states. Since these levels come from the next major neutron shell, the situation is somewhat different from that of the positive-parity states in these nuclei where all the low-lying levels can be described in terms of levels originating from the same major shell: the $3s_{1/2}$, $2d_{3/2}$, $2d_{5/2}$ and $1g_{7/2}$ levels. Since the formalism developed for handling the multilevel calculations may have different properties when discussing these two different situations, we have postponed discussion of the positive-parity states until a later paper.

In sect. 2 then, we shall review the formalism of the interacting boson-fermion model, followed in sect. 3 by the application of the model to the study of the energy spectra of the negative-parity states. For the case where the odd neutron is restricted to occupy only the $1h_{11/2}$ orbital, the results are quite similar to those produced by the triaxial rotor-plus-particle model [3]). We also consider the inclusion of the $2f_{7/2}$ and $1h_{92}$ levels and discuss the effects of this on the low-lying spectra. Finally, in sect. 4, we examine the available information on the electromagnetic properties of these negative-parity states.

## 2. The interacting boson–fermion model

The interacting boson–fermion model [6]) has now been applied in several cases, involving various single-particle orbitals [7–9]). However, the formalism for multilevel calculations has not been elucidated previously, so we shall review it here.

### 2.1. THE HAMILTONIAN

The total hamiltonian can be written as a sum of three parts:

$$H = H_{\mathrm{B}} + H_{\mathrm{F}} + V_{\mathrm{BF}} . \tag{1}$$

The boson hamiltonian, $H_{\mathrm{B}}$, takes the following form [10]):

$$\begin{aligned} H = {} & \varepsilon_{\mathrm{s}}\hat{n}_{\mathrm{s}} + \varepsilon_{\mathrm{d}}\hat{n}_{\mathrm{d}} + 1/2\,u_0[(s^+\times s^+)^{(0)}\times(\tilde{s}\times\tilde{s})^{(0)}]^{(0)} + u_2[(d^+\times s^+)^{(2)}\times(\tilde{d}\times\tilde{s})^{(2)}]^{(0)} \\ & + \sqrt{\tfrac{1}{2}}v_0[(d^+\times d^+)^{(0)}\times(\tilde{s}\times\tilde{s})^{(0)} + (s^+\times s^+)^{(0)}\times(\tilde{d}\times\tilde{d})^{(0)}]^{(0)} \\ & + v_2[(d^+\times d^+)^{(2)}\times(\tilde{d}\times\tilde{s})^{(2)} + (d^+\times s^+)^{(2)}\times(\tilde{d}\times\tilde{d})^{(2)}]^{(0)} \\ & + 1/2\sum_L \sqrt{2L+1}c_L[(d^+\times d^+)^{(L)}\times(\tilde{d}\times\tilde{d})^{(L)}]^{(0)} , \end{aligned} \tag{2}$$

where $\tilde{d}_\mu = (-)^\mu d_{-\mu}$. This represents the most general two-body interaction between s- and d-bosons. There are nine parameters in (2), but if the binding energy of the nucleus is ignored, only six of them are independent. In constructing the odd-mass spectrum, these even core parameters are fixed by fitting the spectrum of the neighboring even-even nucleus. One of the key features of this model is the ability to provide accurate descriptions of the even–even cores, and in fig. 1 we show the

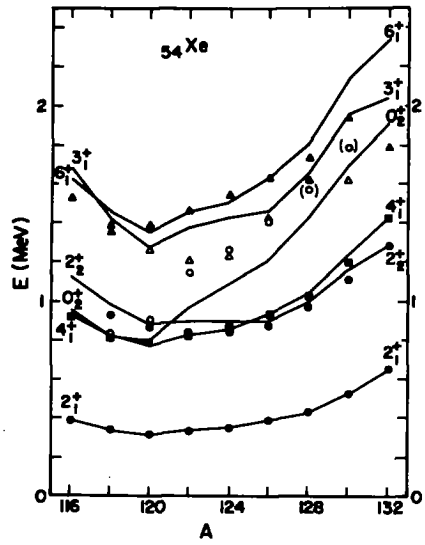


Fig. 1. Excited state energy levels in the even-even xenon isotopes. Experimental levels (points) are from ref. [11]). Open circles indicate $0^+$ states, closed circles indicate $2^+$ states, open triangles indicate $3^+$ states, closed squares indicate $4^+$ states, and closed triangles indicate $6^+$ states.

fits to the even-mass xenon isotopes. The experimental levels (points) are taken from a compilation by Sakai and Gono [11]), and are reproduced quite well by the calculations. Similar results for the even-mass barium isotopes are shown in fig. 2.

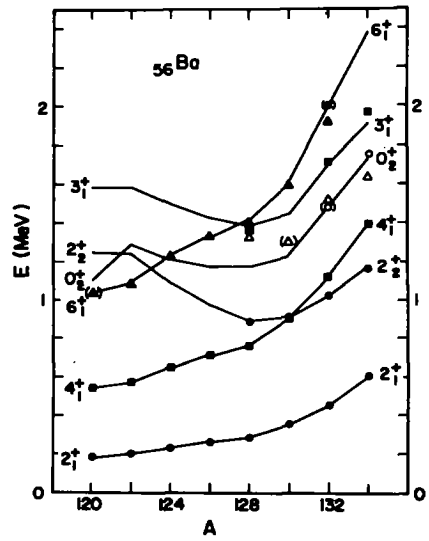


Fig. 2. Excited state energy levels in the even-even barium isotopes. Experimental levels (points) are from ref. [11]), and are plotted as defined in fig. 1.

The fermion hamiltonian, $H_F$, is rather simple, since there is only a single fermion in the problem. It is just the quasi-particle energies:

$$H_F = \sum_j \varepsilon_j \hat{n}_j , \tag{3}$$

where the sum runs over the available single-particle levels. For the case where the odd nucleon occupies only one single-particle orbital, this term adds only an overall shift to the energy spectrum and can be neglected.

Finally, the boson-fermion interaction, $V_{BF}$, we have used in this work is not the most general one, but one suggested by microscopic calculations [12]):

$$V_{BF} = \sum_j A_j [(d^+ \times \tilde{d})^{(0)} \times (a_j^+ \times \tilde{a}_j)^{(0)}]^{(0)} + \sum_{ij} \Gamma_{ij} [\{(s^+ \times \tilde{d} + d^+ \times \tilde{s})^{(2)} + \chi (d^+ \times \tilde{d})^{(2)}\} \times (a_i^+ \times \tilde{a}_j)^{(2)}]^{(0)} + \sum_{ijk} \Lambda_{ij}^k : [(a_i^+ \times \tilde{d})^{(k)} \times (d^+ \times \tilde{a}_j)^{(k)}]^{(0)} : , \tag{4}$$

where $\tilde{a}_{jm} = (-)^{j-m} a_{j-m}$ and the colons in the last term represent the normal ordered product. The three terms represent monopole, quadrupole and exchange interactions, respectively. In a single $j$-orbit limit, such as would be used to describe unique parity states, the summations in (4) go away and we are left with four parameters: $A$, $\Gamma$, $\chi$ and $\Lambda$. The parameter $\chi$ is derived from the boson quadrupole operator, so there are only three free parameters in the single $j$-orbit limit. This simplification makes analysis of the energy spectra much more tractable, and is one we would like to retain in the study of cases where several single-particle levels would be important.

To retain the simplicity of the single $j$-orbit formalism in multilevel situations will, of course, require further assumptions on the $j$-dependence of the interaction parameters. Scholten has analyzed this problem and developed a formalism [12]) based on the BCS equations [13]). The $j$-dependence of the interaction parameters is factored out into single-particle matrix elements, and the intrinsic structure is reflected in BCS occupation probabilities. Explicitly, he finds the following:

$$A_j = A\sqrt{5}(2j+1) , \tag{5a}$$

$$\Gamma_{ij} = \Gamma\sqrt{5}(u_i u_j - v_i v_j)\langle i \| Y^{(2)} \| j \rangle , \tag{5b}$$

$$\Lambda_{ij}^k = -\Lambda 2\sqrt{5/(2k+1)}\beta_{ik}\beta_{kj} , \tag{5c}$$

$$\beta_{ij} = (u_i v_j + u_j v_i)\langle i \| Y^{(2)} \| j \rangle . \tag{5d}$$

The $u_j$ and $v_j$ in (5) are the occupation probabilities. To arrive at values for these parameters in practice requires a set of single-particle energies, $E_j$, and the pairing gap energy, $\Delta$. With this information, one can solve the gap equations:

$$\varepsilon_j = [(E_j - \lambda)^2 + \Delta^2]^{1/2} , \tag{6a}$$

$$v_j^2 = \tfrac{1}{2}[1 - (E_j - \lambda)/\varepsilon_j] , \tag{6b}$$

subject to the constraint that the total number of valence nucleons be conserved:

$$n = \sum_j v_j^2 (2j+1) . \tag{7}$$

The $u_j$ can then be obtained from the simple relation: $u_j^2 + v_j^2 = 1$. Thus with some additional physical input, the simplicity of the single $j$-orbit formalism can be retained.

## 2.2. ELECTROMAGNETIC OPERATORS

In general, the form of the electromagnetic transition operators can be written as follows:

$$T^{(L)} = e_B^{(L)} T_B^{(L)} + e_F^{(L)} \sum_{ij} T_{ij}^{(L)} (a_i^+ \times \tilde{a}_j)^{(L)} . \tag{8}$$

The effective charges of the boson operators, $e_B^{(L)}$, are fixed for all isotopes by fitting to transitions in the even–even cores. In this paper, we shall restrict our attention to the study of the electric quadrupole and magnetic dipole transitions and moments. The boson E2 transition operator, $T_B^{(E2)}$, can be written as follows:

$$T_B^{(E2)} = (s^+ \times \tilde{d} + d^+ \times \tilde{s})^{(E2)} + \chi (d^+ \times \tilde{d})^{(2)} . \tag{9}$$

The effective boson charge, $e_B$, was fixed to be $e_B = 0.13\, e \cdot \mathrm{b}$, by comparison with measured $B(\mathrm{E2} : 0_1^+ \to 2_1^+)$ values in the even-mass barium isotopes. In fig. 3, we compare the predicted $B(\mathrm{E2} : 0_1^+ \to 2_1^+)$ values in the even-mass barium isotopes with the experimental values [14]). The boson M1 transition operator, $T_B^{(M1)}$, can be written as follows:

$$T_B^{(M1)'} = g_B (d^+ \times \tilde{d})^{(1)} . \tag{10}$$

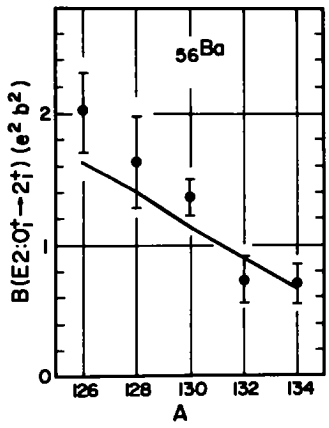


Fig. 3. $B(\mathrm{E2}: 0_1^+ \to 2_1^+)$ values in the even-mass barium isotopes. The experimental data are from ref. [14]).

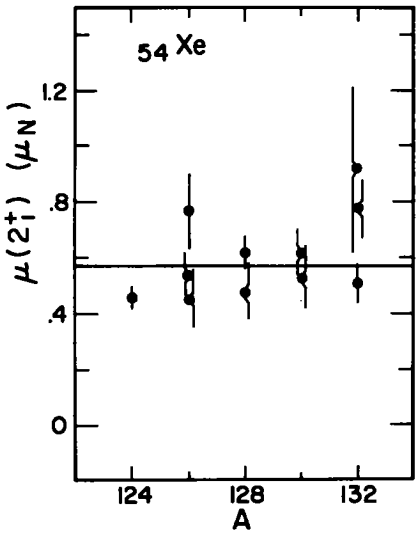


Fig. 4. Magnetic dipole moments of $2_1^+$ states in the even-mass xenon isotopes. The experimental data are from ref. [15]).

We have fixed the boson effective $g$-factor, $g_B = 0.14\ \mu_N$, by comparing with the observed magnetic moments of $2_1^+$ states in the xenon isotopes. These results are shown in fig. 4, where the experimental values of the moments have been taken from ref. [15]). This fixes the boson part of the electromagnetic operators, and leaves only the specification of the fermion effective charges.

In the single $j$-orbit limit, the summation in (8) goes away and only the fermion effective charges are left. In practice, these strengths will be fixed by comparison with experimental data as was done for the boson parts of the operators. However, in the multilevel case, it is possible to arrive at a single-particle estimate of the effective charges which precludes fitting another parameter.

For electric multipoles, the fermion single-particle transition operator is given by the following [16]):

$$T_m^{(EL)} = r^L Y_m^{(L)}(\theta, \phi)\,, \tag{11}$$

which has matrix elements between single-particle states of the following form:

$$\langle i \| T^{(EL)} \| j \rangle = \langle r^L \rangle \langle i \| Y^{(L)} \| j \rangle\,. \tag{12}$$

Equating matrix elements of operators (8) and (11) between single-particle states implies that:

$$T_{ij}^{(L)} = -\langle r^L \rangle \langle i \| Y^{(L)} \| j \rangle / \sqrt{(2L+1)}\,. \tag{13}$$

However, if we also take into account the intrinsic structure reflected in the BCS

occupation probabilities, the fermion transition operator becomes the following:

$$T_{\mathrm{F}}^{(\mathrm{E}L)} = -\langle r^L\rangle/\sqrt{(2L+1)}\sum_{ij}(u_iu_j - v_iv_j)\langle i\|Y^{(L)}\|j\rangle(a_i^+ \times \tilde{a}_j)^{(L)}\,. \tag{14}$$

The radial matrix elements $\langle r^L\rangle$ we shall usually assume to be constant for all levels in a given major shell and consequently absorb them into the effective charges. For the odd neutron nuclei under consideration in this paper, this implies that $e_{\mathrm{F}} = \langle r^2\rangle e_{\mathrm{n}}$, for the E2 operator.

The same analysis can be applied to the magnetic multipole operators, but the problem is slightly more complicated, owing to the more complicated structure of the fermion single-particle operator [16]):

$$T_m^{(\mathrm{M}L)} = \nabla[r^L Y_m^{(L)}(\theta,\phi)]\left[\frac{2g_l}{(L+1)}\mathbf{l} + g_s\mathbf{s}\right]. \tag{15}$$

Rather than repeat the process, we give only the result:

$$\begin{aligned} T_{\mathrm{F}}^{(\mathrm{M}L)} = {} & -\langle r^{L-1}\rangle\sqrt{L(2L+1)}\sum_{ij}(u_iu_j + v_iv_j)\sqrt{(2i+1)(2j+1)}\langle l_i\|Y^{(L-1)}\|l_j\rangle \\ & \times\left[\frac{2g_l}{(L+1)}(-)^{i+l_i+1/2}\sqrt{j(j+1)(2j+1)^2}\begin{Bmatrix} L-1 & 1 & L \\ j & i & j\end{Bmatrix}\begin{Bmatrix} l_i & i & \frac{1}{2} \\ j & 1 & L-1\end{Bmatrix}\right. \\ & \left. + [g_s - 2g_l/(L+1)]\sqrt{\tfrac{3}{2}}\begin{Bmatrix} l_i & \frac{1}{2} & i \\ l_j & \frac{1}{2} & j \\ L-1 & 1 & L\end{Bmatrix}\right](a_i^+ \times \tilde{a}_j)^{(L)}\,. \end{aligned} \tag{16}$$

For magnetic dipole transitions, the effective fermion $g$-factor remains a free parameter, but the nucleon $g$-factors, $g_l$ and $g_s$, are taken to have their usual values.

## 3. Negative-parity states in Xe and Ba

The high-spin, negative-parity states in the light isotopes of xenon and barium have been extensively studied in recent years. This large body of data results in rigid constraints on any analysis.

### 3.1. SINGLE $j$-ORBIT APPROXIMATION

As a first approximation in studying the high-spin, negative-parity states in the light isotopes of xenon and barium, we restrict the odd neutron to the $1h_{11/2}$ orbital. With this assumption, the hamiltonian takes on the simple form we discussed in the previous section. In fig. 5, we show the results of our calculations for the odd-mass xenon isotopes. The boson–fermion interaction parameters used in these calculations are listed in table 1. The spectra have been decomposed for clarity,

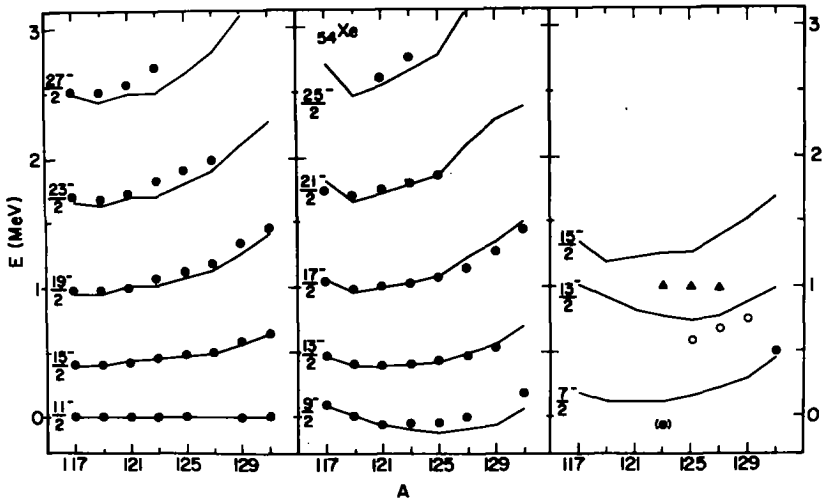


Fig. 5. Energy levels in the odd-mass xenon isotopes. Experimental data (points) are from refs. [17–23]), and are plotted so that the energy of the $\frac{11}{2}^-_1$ state is zero.

since several of the levels are nearly degenerate. The experimental levels (points) have been taken from several sources[17–23]). Overall, one sees rather smooth trends in the positions of levels, and this is reflected in the calculated energies as well. In fig. 6, we show a detailed comparison of the isotopes $^{119}$Xe and $^{121}$Xe. Most

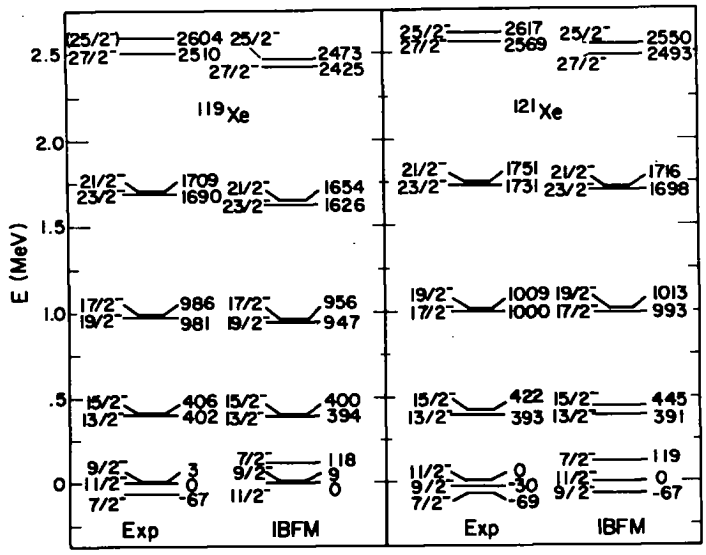


Fig. 6. Detailed level schemes for the isotopes $^{119}$Xe and $^{121}$Xe. The experimental data are from refs. [20,21]), and are plotted with the $\frac{11}{2}^-_1$ state at zero energy.

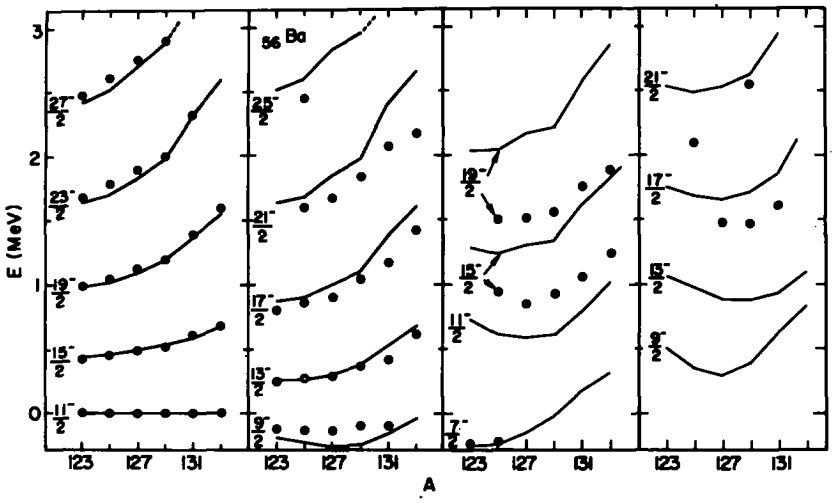


Fig. 7. Energy levels in the odd-mass barium isotopes. Experimental levels (points) are from refs. [24–28]).

impressive about the results in these two isotopes is the reproduction of the observed pairs of levels: $\frac{13}{2}-\frac{15}{2}$, $\frac{17}{2}-\frac{19}{2}$, etc. The reversal of the ordering of the $\frac{17}{2}-\frac{19}{2}$ doublet is even reproduced. This is particularly noteworthy since the calculations represent a strongly coupled system. The $\frac{9}{2}^-$ state observed at 3 keV in $^{119}$Xe, for example, must arise from the multiplet based on the $2_1^+$ state in the even core nucleus. Not all the members of this multiplet are observed, but the energy splitting between the extreme members is some 473 keV, which is comparable to the

TABLE 1

Hamiltonian parameters for the single $j$-orbit calculations (in units of MeV)

| Isotope | $A$ | $\Gamma$ | $\Lambda$ |
|---|---|---|---|
| $^{117}$Xe | −0.150 | 0.30 | 0.757 |
| $^{119}$Xe | −0.050 | 0.15 | 0.792 |
| $^{121}$Xe | −0.050 | −0.15 | 0.828 |
| $^{123}$Xe | −0.150 | −0.30 | 0.865 |
| $^{125}$Xe | −0.275 | −0.50 | 0.901 |
| $^{127}$Xe | −0.375 | −0.63 | 0.943 |
| $^{129}$Xe | −0.470 | −0.70 | 0.980 |
| $^{131}$Xe | −0.500 | −0.75 | 0.980 |
| $^{123}$Ba | −0.050 | 0.10 | 1.21 |
| $^{125}$Ba | −0.150 | −0.10 | 1.21 |
| $^{127}$Ba | −0.050 | −0.40 | 1.21 |
| $^{129}$Ba | −0.100 | −0.60 | 1.21 |
| $^{131}$Ba | −0.200 | −0.80 | 1.21 |
| $^{133}$Ba | −0.250 | −1.00 | 1.32 |

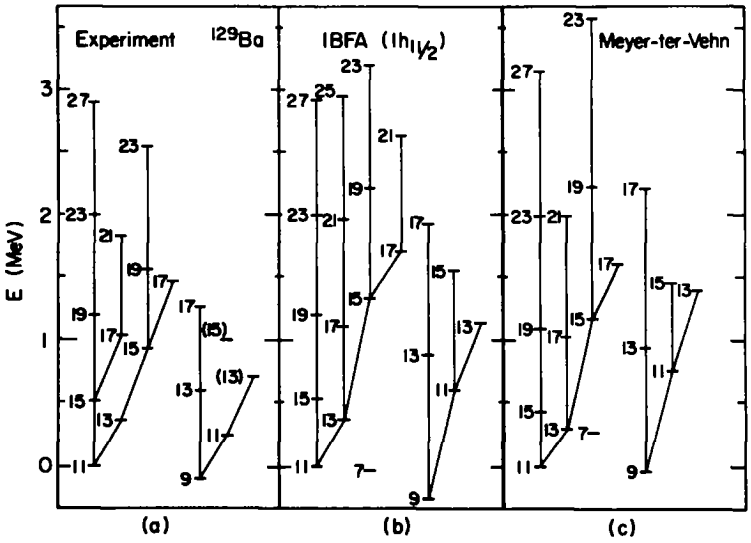


Fig. 8. (a) Experimental levels [25]) in $^{129}$Ba. (b) Theoretical level scheme, incorporating the $1h_{11/2}$ orbital only. (c) Triaxial rotor-plus-particle predictions [25]) for the levels in $^{129}$Ba.

excitation energy. Indeed, in $^{119}$Xe, the $\frac{7}{2}^-$ member of this multiplet becomes the base state. This last fact is not one reproduced by the calculations, and is a point to which we shall return shortly.

The situation is much the same in the barium isotopes. The results of our calculations for these nuclei are shown in fig. 7; the experimental levels taken from refs. [24–28]). The boson–fermion interaction parameters for these calculations are listed in table 1. Of particular interest is the isotope $^{129}$Ba, for which the experimental spectrum is highly developed [25]). In fig. 8a, we show a more detailed experimental spectrum of $^{129}$Ba, where the lines connecting the states indicate the primary decay modes. The results of our calculations are shown in fig. 8b, where the differences between experimental and theoretical levels become more pronounced as one moves away from the yrast band. Interestingly enough, this is much the same result as was found in a triaxial rotor-plus-particle calculation [25]) for this nucleus, which we show in fig. 8c. The models have quite different origins, but nevertheless produce nearly identical results for the observed levels in $^{129}$Ba. We should note, however, that since the triaxial rotor-plus-particle model includes a rigid core, whereas the cores included in this model are rather soft, we would expect the models to differ for the totally anti-aligned states.

There is some ingredient missing from the calculations which will permit the description of these states away from the yrast band. The bands built on the $\frac{9}{2}^-_1$ state in $^{129}$Ba are not well-reproduced, and the $\frac{7}{2}^-_1$ states are observed to lie lower

TABLE 2

BCS parameters for the multilevel calculations (in units of MeV)

| | $3s_{1/2}$ | $2d_{3/2}$ | $2d_{5/2}$ | $1g_{7/2}$ | $1h_{11/2}$ | $2f_{7/2}$ | $1h_{9/2}$ |
|---|---|---|---|---|---|---|---|
| $E_j$ | −0.334 | 0.0 | −1.654 | −2.429 | −0.434 | 3.0 | 3.12 |
| $^{125}Xe$ | | | | | | | |
| $\varepsilon_j$ | 1.081 | 1.171 | 1.599 | 2.235 | 1.074 | 3.631 | 3.746 |
| $v_j^2$ | 0.438 | 0.300 | 0.871 | 0.939 | 0.484 | 0.022 | 0.021 |
| $^{127}Xe$ and $^{129}Ba$ | | | | | | | |
| $\varepsilon_j$ | 1.068 | 1.098 | 1.758 | 2.420 | 1.080 | 3.426 | 3.540 |
| $v_j^2$ | 0.537 | 0.383 | 0.898 | 0.949 | 0.582 | 0.025 | 0.023 |
| $^{129}Xe$ and $^{131}Ba$ | | | | | | | |
| $\varepsilon_j$ | 1.099 | 1.057 | 1.935 | 2.618 | 1.130 | 3.212 | 3.326 |
| $v_j^2$ | 0.637 | 0.484 | 0.919 | 0.958 | 0.677 | 0.028 | 0.026 |
| $^{133}Ba$ | | | | | | | |
| $\varepsilon_j$ | 1.189 | 1.073 | 2.153 | 2.855 | 1.239 | 2.965 | 3.078 |
| $v_j^2$ | 0.736 | 0.606 | 0.937 | 0.965 | 0.766 | 0.032 | 0.030 |

than our calculations would indicate. The reason for these discrepancies could be due to the fact that we have ignored other fermion degrees of freedom. In this mass region, the $2f_{7/2}$ and $1h_{9/2}$ levels could conceivably contribute to the low-lying structure in these negative-parity states, so we shall examine the effects of incorporating these levels.

### 3.2. MULTILEVEL CALCULATIONS

The BCS parameters must first be established, which requires a set of single-particle energies, $E_j$, and the pairing gap energy, $\Delta$. The single-particle energies for levels in the 50–82 neutron shell were taken from $^{131}$Sn [ref. [15])] and the $2f_{7/2}$ and $1h_{9/2}$ levels were placed about 3 MeV higher [29]). The derived quasi-particle energies, $\varepsilon_j$, and occupation probabilities, $v_j$, are listed in table 2 and the boson-fermion interaction parameters in table 3. With these values of the parameters, we then recalculated the energy spectra of the negative-parity states.

The results of these three-level calculations for the isotopes $^{125-129}$Xe are shown in fig. 9. The spectrum of $^{125}$Xe, in particular, shows a great deal of improvement in the agreement between states away from the yrast band. The situation is also improved in the barium isotopes, as is evidenced by fig. 10, where we have reproduced our results for the isotopes $^{129-133}$Ba.

Where the single $j$-orbit calculations were able to reproduce the trends in the data, it would appear that these three-level calculations are able to reproduce the observed spectra with great accuracy. This is illustrated quite nicely by our results

TABLE 3

Hamiltonian parameters for the multilevel calculations (in units of MeV)

| Isotope | $A$ | $\Gamma$ | $\Lambda$ |
|---|---|---|---|
| $^{125}$Xe | −0.30 | 0.65 | 1.30 |
| $^{127}$Xe | −0.35 | 0.85 | 1.20 |
| $^{129}$Xe | −0.30 | −0.90 | 0.75 |
| $^{129}$Ba | −0.35 | 0.85 | 1.50 |
| $^{131}$Ba | −0.40 | −0.93 | 1.30 |
| $^{133}$Ba | −0.50 | −1.20 | 0.70 |

in $^{129}$Ba, which we show in fig. 11. Now not only is the yrast band reproduced, but the various side bands are reproduced as well. The arrows connecting states in fig. 11 indicate the primary decay modes, which we shall come to in the next section. While there appear to be a few discrepancies in the fits, the overall conclusion to which we are led is that these other fermion degrees of freedom do indeed play a

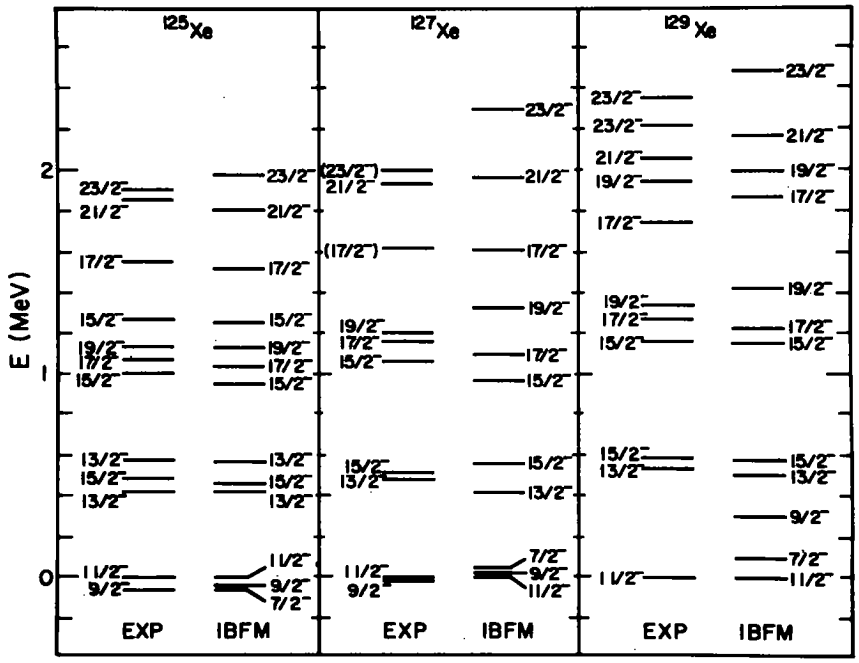


Fig. 9. Energy levels in $^{125-129}$Xe. Experimental data are from refs. [17–19,23]). The theoretical calculations include the $1h_{11/2}$, $2f_{7/2}$ and $1h_{9/2}$ single-particle levels.

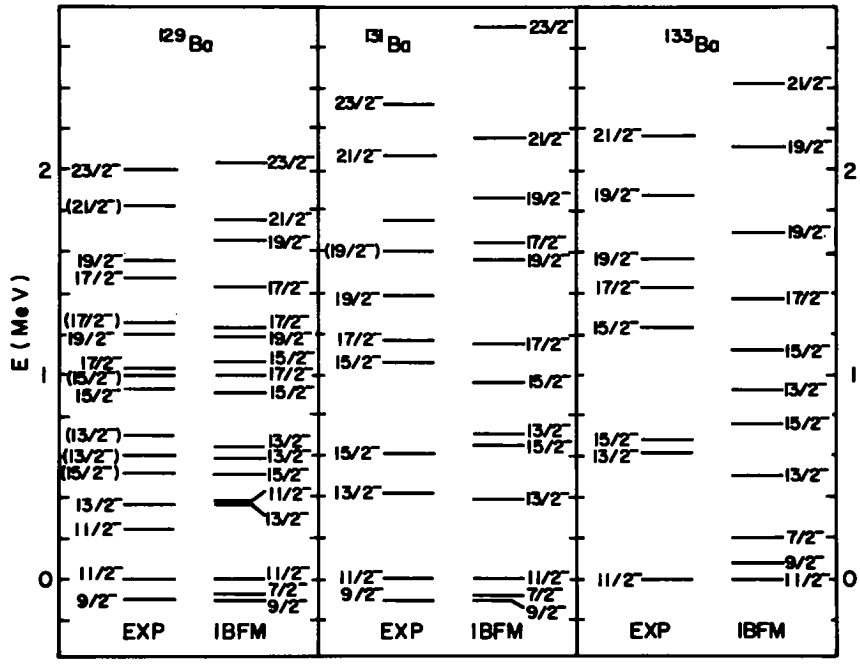


Fig. 10. Energy levels in $^{129-133}$Ba. Experimental data are from refs. [24,25]). The theoretical calculations include the $1h_{11/2}$, $2f_{7/2}$ and $1h_{9/2}$ single-particle levels.

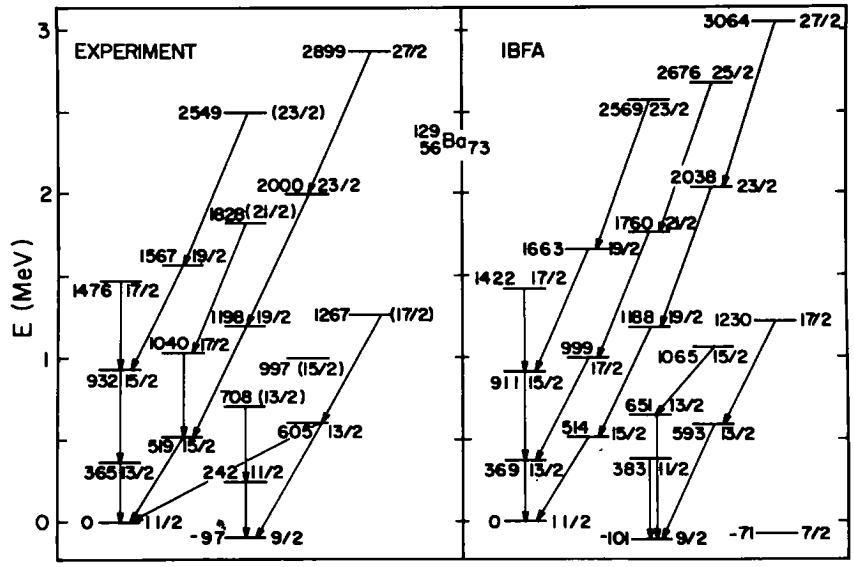


Fig. 11. Energy levels in $^{129}$Ba. Experimental data are from ref. [25]). The theoretical calculations include the $1h_{11/2}$, $2f_{7/2}$ and $1h_{9/2}$ single-particle levels.

large role in determining the structure of the low-lying spectra. The energies of states are, of course, not as sentitive to the details of the model wave functions as are the electromagnetic transitions, so before we can state that we have provided a description of these states, we must first examine the electromagnetic properties.

## 4. Electromagnetic transitions

The high-spin negative-parity states we have considered in this paper have been studied experimentally primarily via heavy ion, $xn$ techniques. Unfortunately, it is difficult to extract information about the electromagnetic transition matrix elements from these experiments, and as these states cannot be easily reached via other means, much of the detailed experimental information necessary to compare with our calculations is unavailable. For the positive-parity states in these nuclei, some of this information does exist, and we shall comment on this in a subsequent paper. For the moment, however, we shall focus our attention on the isotope $^{129}$Ba, for which there is some experimental information on which we can comment.

### 4.1. E2 TRANSITIONS

For the single $j$-orbit calculation, the fermion effective charge was chosen to be $e_F = -0.34\, e \cdot \mathrm{b}$, by fixing the quadrupole moment of the $\frac{11}{2}^-_1$ state in $^{129}$Ba [ref. [14])]. For the three-level calculation, we took the harmonic oscillator value for the radial matrix element: $\langle r^2 \rangle = (\mathrm{N} + \frac{3}{2})\hbar/M\omega$. Using $e_n = 0.5e$, leads to a value of $e_F = -0.17\, e \cdot \mathrm{b}$, where the sign arises from the hole-like nature of the odd neutron. With these charges established, the E2 transition operator (8) is fixed, and we can now compute $B(\mathrm{E2})$ values.

Nominally, we would expect the boson transitions to dominate the E2 matrix elements, since they represent the collective part of the problem. The E2 transitions of a weakly-coupled boson–fermion system would tend to populate final states in which the angular momentum coupling of the odd fermion is not changed. Hence a $\Delta J = 2$ structure, reflecting the quadrupole nature of the bosons would arise. We have remarked previously, however, that these systems we are studying are not weakly coupled, so there could be large deviations from the $\Delta J = 2$ rule. For transitions between band heads, it is possible that the single-particle transitions play some larger role.

In table 4, we list the experimental $B(\mathrm{E2})$ branching ratios [25]) for the isotope $^{129}$Ba, along with the results of the single $j$-orbit and three-level calculations. In general, the single $j$-orbit calculation tends to generate a $\Delta J = 2$ structure. Experimentally, though, the situation is the opposite. The $\frac{15}{2}^-_1$ level, for example, decays predominantly to the $\frac{13}{2}^-_1$ state, not the $\frac{11}{2}^-_1$. The single-orbit calculation would make this ratio about unity, indicating that the mixing of the bands is strong.

TABLE 4

$B$(E2) branching ratios in $^{129}$Ba

| Transitions | Exp | IBFM | |
|---|---|---|---|
| | | 1-level | 3-level |
| $\frac{13}{2}^-_1 \rightarrow \frac{9}{2}^-_1$ / $\frac{13}{2}^-_1 \rightarrow \frac{11}{2}^-_1$ | 0.06–0.08 | 1.43 | 0.14 |
| $\frac{15}{2}^-_1 \rightarrow \frac{11}{2}^-_1$ / $\frac{15}{2}^-_1 \rightarrow \frac{13}{2}^-_1$ | 0.03–0.23 | 1.2 | 3.50 |
| $\frac{17}{2}^-_1 \rightarrow \frac{13}{2}^-_1$ / $\frac{17}{2}^-_1 \rightarrow \frac{15}{2}^-_1$ | 1.03–12.7<br>0.19–0.24 | 5.4 | 2.30 |
| $\frac{19}{2}^-_2 \rightarrow \frac{15}{2}^-_2$ / $\frac{19}{2}^-_2 \rightarrow \frac{17}{2}^-_1$ | 0.95–3.13 | 10.0 | 1.49 |
| $\frac{13}{2}^-_2 \rightarrow \frac{9}{2}^-_1$ / $\frac{13}{2}^-_2 \rightarrow \frac{11}{2}^-_1$ | 1.36–8.20 | 0.05 | 0.17 |

However, the mixing appears not to be the one required to explain the experimental decays.

The situation is not clear in the decay of the $\frac{17}{2}^-_1$ state, since there is an experimental ambiguity in the branching ratio. The remaining ratios are between members of different bands, and are presumably quite sensitive to the model wave functions. The simple description of these states provided by the single $j$-orbit approximation appears not to be adequate, which apparently is also the case in the triaxial rotor-plus-particle model [25]).

There is indeed some improvement in the three-level calculations over that of the single $j$-orbit limit, but it is perhaps not as much as we could have hoped. The most dramatic improvement occurs in the decay of the $\frac{13}{2}^-_1$ state, for which the three-level calculation provides an order-of-magnitude improvement. However, the $\frac{15}{2}^-_1 \rightarrow \frac{11}{2}^-_1$ transition is now even stronger, relative to the $\frac{15}{2}^-_1 \rightarrow \frac{13}{2}^-_1$ transition, than in the single $j$-orbit case. Clearly something far more subtle than we had envisioned is the case in these states. However, without more detailed information about the transitions among these states it is not clear where the model has difficulty, or where improvements need to be made.

### 4.2. M1 MOMENTS

Since the E2 transitions are dominated by the boson degrees of freedom, it would be illuminating to study the M1 transitions in these nuclei to probe the single-particle degrees of freedom. This would perhaps clarify some of the earlier difficulties. However, the only data on the magnetic dipole properties of these negative-parity states are moments of the $\frac{11}{2}^-_1$ states. We list these in table 5, along with the

TABLE 5
Magnetic dipole moments of $\frac{11}{2}^-$ states (in units of $\mu_N$)

| Isotope | Exp | IBFM | |
|---|---|---|---|
| | | 1-level | 3-level |
| $^{129}$Xe | −0.847 (28) | −0.83 | −1.09 |
| $^{131}$Xe | −0.8 (1) | −0.83 | |
| $^{133}$Ba | −0.91 (4) | −0.83 | −1.04 |

predictions of the two theoretical calculations. For the single $j$-orbit calculation, the effective fermion $g$-factor was chosen to be $g_F = 0.9$, by fitting to the moment in $^{129}$Xe. In the multilevel case, we chose $g_F = 0.6$, which is a value consistent with the quenching of the spin magnetic moments for other nuclei in this mass region [23,29]). Since there are few data, it is not possible to make any general statements about the importance of the additional single-particle degrees of freedom on the M1 transitions. The single $j$-orbit calculation produces values of the moments which are closer to the experimentally observed ones, but this is, of course, due to the fact that we fitted the fermion effective $g$-factor to these moments. The three-level calculation produces values for these moments which are nonetheless reasonable.

## 5. Summary

The interacting boson–fermion model provides a framework within which it is possible to describe the structure of the low-lying collective states in transitional, odd-mass nuclei. In the single $j$-orbit approximation, the model provides a description of the unique-parity states that we have examined which is comparable to that of the triaxial rotor-plus-particle model [25]). However, the formalism exists to perform calculations in which several single-particle degrees of freedom are involved, and as we have seen, these additional levels can dramatically affect the structure of the low-lying spectrum. Given the dramatic improvement in the spectrum of $^{129}$Ba, for example, with the adddition of the $h_{9/2}$ and $f_{7/2}$ levels, it would seem that even for the study of unique-parity states, it is important to include other levels. Unfortunately, the detailed experimental information on electromagnetic transitions necessary to fully test the model is lacking. On the surface, it would appear that it is now possible to provide detailed descriptions of the properties of the collective states in these transitional, odd-mass nuclei, although we have not fully resolved this problem in this paper.

The author would like to thank Professor Franco Iachello for many useful discussions and Professors Dave Fossan and John Wood and Dr. Jean Gizon for

their kind assistance with the experimental data. This work has been funded by USDOE Contract No. DE-AC02-76ER03074.

## References

1) S.G. Nilsson, Matt. Fys. Medd. Dan. Vid. Selsk. **29**, No. 16 (1955)
2) A. Bohr, Matt. Fys. Medd. Dan. Vid. Selsk. **26**, No. 14 (1952);
A. Bohr and B. Mottelson, Matt. Fys. Medd. Dan. Vid. Selsk. **27**, No. 16 (1953)
3) J. Meyer-ter-Vehn, Nucl. Phys. **A249** (1975) 111
4) G. Leander, Nucl. Phys. **A273** (1976) 286
5) H. Toki and A. Faessler, Nucl. Phys. **A253** (1975) 231
6) A. Arima and F. Iachello, Phys. Rev. **C14** (1976) 761
7) F. Iachello and O. Scholten, Phys. Rev. Lett. **43** (1979) 679
8) U. Kaup, A. Gelberg, P. von Brentano and O. Scholten, Phys. Rev. **C22** (1980) 1738
9) G. LoBianco, N. Molho, A. Moroni, A. Bracco and N. Blasi, J. of Phys. **G7** (1981) 219
10) A. Arima and F. Iachello, Ann. of Phys. **99** (1976) 253
11) M. Sakai and Y. Gono, Atomic and Nucl. Data Tables **20** (1977) 441
12) O. Scholten, Ph. D. thesis, U. Groningen, 1980, unpublished
13) J. Bardeen, L. N. Cooper and R. Schrieffer, Phys. Rev. **108** (1957) 1175
14) K. Bekk, A. Andl, S. Goring, A. Hanser, G. Nowicki, H. Rebel and G. Shatz, Z. Phys. **A291** (1979) 219
15) C. M. Lederer and V.S. Shirley, ed., Table of Isotopes, 7th edition (Wiley, New York, 1977)
16) A. de-Shalit and I. Talmi, Nuclear shell theory (Academic Press, New York, 1963)
17) I. Rezanka, A. Kerek, A. Luukko and C.J. Herrrlander, Nucl. Phys. **A141** (1970) 130
18) A. Gizon and J. Gizon, Z. Phys. **A289** (1978) 59
19) H. Helppi, J. Hattula and A. Luukko, Nucl. Phys. **A332** (1979) 183
20) V. Barci, A. Gizon, J. Crawford, J. Genevy, J. Gizon and A. Plochocki, Proc. Int. Conf. on nuclei far from stability, Helsingør, Denmark, to be published (1981)
21) P. Chowdhury, U. Garg, T.P. Sjoreen and D.B. Fossan, Phys. Rev. **C23** (1981) 733
22) A. Luukko, J. Hattula, H. Helppi, O. Knuuttila and F. Donau, Nucl. Phys. **A357** (1981) 319
23) H. Helppi, J. Hattula, A. Luukko, M. Jaaskelainen and F. Donau, Nucl. Phys. **A357** (1981) 333
24) J. Gizon, A. Gizon and D.J. Horen, Nucl, Phys. **A252** (1975) 509
25) J. Gizon, A. Gizon and J. Meyer-ter-Vehn, Nucl. Phys. **A277** (1977) 464
26) J. Gizon and A. Gizon, Z. Phys. **A281** (1977) 99
27) J. Gizon and A. Gizon, Z. Phys. **A285** (1978) 259
28) N. Yoshikawa, J. Gizon and A. Gizon, J. de Phys. **40** (1979) 209
29) A. Bohr and B. Mottelson, Nuclear structure, vol. I (Benjamin, New York, 1969)